Evidence of 'microscopic bubbles' and a new diffusion mechanism for amorphous alloys

2010 J. Phys.: Condens. Matter 22 035401

(http://iopscience.iop.org/0953-8984/22/3/035401)

J. Phys.: Condens. Matter **22** (2010) 035401 (5pp) doi:10.1088/0953-8984/22/3/035401

Evidence of 'microscopic bubbles' and a new diffusion mechanism for amorphous alloys

P K Hung, P H Kien and L T Vinh

Department of Computational Physics, Hanoi University of Technology, 1 Dai Co Viet, Hanoi, Vietnam

E-mail: pkhung@fpt.vn

Received 25 October 2009, in final form 26 November 2009
Published 21 December 2009
Online at stacks.iop.org/JPhysCM/22/035401

Abstract

Simulation of the diffusion mechanism in amorphous alloys is carried out using three statistical relaxation models $Fe_{80}B_{20}$ with 10^5 atoms. We found for the first time that the simulated models contain a large number of vacancy bubbles, which could be a diffusion vehicle such as a vacancy, as in the case of diffusion in a crystal. The numbers of these vacancy bubbles vary from 2.8×10^{-3} to 1.245×10^{-2} per atom depending on the relaxation degree. Diffusion coefficients have been calculated via the vacancy bubbles and they are very consistent with experiment. The relaxation effect is also studied and interpreted as a result of vacancy-bubble annihilation during thermal annealing.

1. Introduction

It is well established for certain amorphous alloys (AMA) [1–9] that the diffusion coefficient of tracer atoms in well-relaxed specimens decreases compared to as-quenched ones. Usually, this effect has been interpreted as the existence of quasi-vacancies in super-saturation. During thermal annealing these defects are mobile and their super-saturation decreases as a result of 'quasi-vacancies' and 'free volume' annihilations. Hence, the diffusivity in as-quenched AMAs is reduced as a function of time until the relaxation is over and the diffusion coefficient reaches its final value. In the well-relaxed state, conversely, the tracer atoms diffuse, not with the aid of quasi-vacancies, but via the collective movement of a group of neighboring atoms. However, the experimental measurements [10–17] on the isotope effect, pressure dependence and irradiation-enhanced diffusivity are sometimes in contradiction to the prediction of the diffusion mechanisms just described. In addition to these, the definition of the quasi-vacancy is not clear. Furthermore, analyzing the creep and diffusion data indicates that the vacancy-type defect is not the sole solution to satisfy the available experimental data. Molecular dynamic (MD) simulations, on the other hand, reveal the disappearance of vacancies after their introduction into the MD model and then relaxation in 10^{-10} s [18, 19] i.e. the vacancies are unstable in an amorphous matrix. Closer inspection of the MD model found a continuous spectrum of spherical voids [20], but their sizes are less than the atomic size. As regards the collective atomic jumps, the 'free volume' theory, extended from that for a simple liquid, and the 'two-level states' theory are also employed to interpret the specific behavior of diffusion in AMAs [17, 22]. In accordance with the bond deficiency model, several atoms (about 10 or more) move such that one among them displaces over a large distance [21]. Applying this model to Zr–Ti and Ti–Ni systems gives a good agreement with experiment for the size effect of diffusing atoms. However, as noticed in [21, 23, 24], none of the models mentioned could properly interpret the available experimental observations, and the diffusion mechanism of tracer atoms in AMA is still not well understood.

In this paper, an attempt is made to address the role of 'microscopic bubbles' for diffusion in AMAs. This diffusion vehicle is found for the first time in our simulated models. Consequently, a new diffusion mechanism may occur due to the contribution of these bubbles and the relaxation effect must also relate to them. Therefore, this motivates us to carry out a systematic study of these bubbles in order to shed new light on the diffusion mechanism of tracer atoms in AMAs.

2. Calculation procedure

The molecular dynamic method is proven to be a valuable tool for studying the structure and formation of AMA, but it

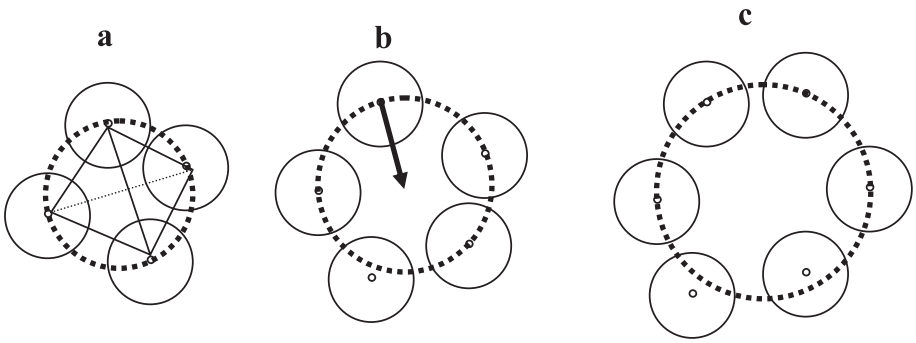

Figure 1. The schematic illustration of the bubbles in the simulated model: (a) the simplest structural unit where four neighboring atoms form a tetrahedron; (b) and (c) the bubbles with 5 and 6 atoms respectively; the dot-sided circle represents a CST. The arrow denotes the displacement vector of DA.

requests very long computing times to construct a large model. In this work we employ the statistic relaxation method (SR) to prepare a model $Fe_{80}B_{20}$ of 10^5 atoms, because it is cheaper to compute. In addition, the SR method also enables us to construct models in different metastable states and to quickly relax the system upon introducing the atomic jumps. The SR method is in fact the molecular dynamic method in the limit of zero temperature, e.g. the kinetic energy is equal to zero and the volume is constant. Accordingly, each atom in the system moves in the direction of the force acting on the given atom from all the remaining ones by a length dr. This movement is repeated many times until the system reaches equilibrium. The averaged potential energy per atom is determined by

$$U = \frac{1}{N_{\mathrm{Atom}}} \sum_{i<j} \varphi(r_{ij}), \tag{1}$$

where r_{ij} is the distance between the ith and jth atoms; $\varphi(r_{ij})$ is the pair interaction potential; N_{Atom} is the number of atoms. More details on the SR method can be found elsewhere [20, 25, 32]. The simulation was performed on a cluster system consisting of 50 PC nodes at the High Performance Center, Hanoi University of Technology.

The initial configuration is generated by randomly placing all atoms in a cube with periodic boundary conditions. The effective pair potential of [20] is used and the density is adopted from a real amorphous alloy ($\sim$7.4 g cm^{-3}). This sample is treated over 10^6 SR steps to reach the equilibrium state. The SR step length is equal to 0.01 Å. The validity of the constructed model has been tested in that it reproduces the pair distribution functions (PDF) well. Hereafter, this model is called model A. To study the effect of relaxation, we prepare two additional models (model B and C) with the same density as model A, but for which the potential energy is lower. Model B was prepared by relaxing model A with a SR step length of 0.4 Å within 100 SR steps. This is like shaking many times the atomic arrangement in model A. Then we relax the obtained samples with the SR step length 0.01 Å until the system reaches a new equilibrium. This procedure is repeated many times such that the potential energy of the model attains the desired value. The model C was obtained by an analogous procedure.

Figure 1 schematically illustrates 'microscopic bubbles' in the amorphous structure. Four nearest neighboring atoms form a tetrahedron. If we built a circumsphere of this tetrahedron (CST), then this CST may contain some atoms inside. The atoms inside the CST are denoted as the ones that are located from a center of CST at a distance less than $R_{\mathrm{B}} - 0.1$ Å. In the following, we consider just the CST which does not contain any atoms. Let R_{B} and n_{B} to be the radii of the CST (radii of the bubble) and the number of atoms near the surface of the CST, respectively. The atoms on the surface of the CST are the ones that are located from the center of CST at a distance in the range of $R_{\mathrm{B}} \pm 0.1$ Å. Figure 1 presents three CSTs with $n_{\mathrm{B}} = 4$, 5 and 6. The first one is the simplest structural unit (figure 1(a)). The 'microscopic bubble' is denoted as that CST which attains n_{B} greater than 4. Probably, these bubbles have been formed due to the rapid cooling process. They represent a defect in the amorphous structure. One of most important properties of the bubbles is that they have a larger empty space inside the CST in comparison with the simplest structural unit (see figure 1). If one of the atoms located near the CST surface could jump into the CST, then we observe an elementary diffusion process similar to the movement in the opposite direction between an atom and a vacancy in crystal.

3. Results and discussion

The structural characteristics of the constructed models are summarized in table 1. They are very close to the simulation data in [25] and reproduce well the diffraction experimental data from [26–28]. The PDFs for model A, shown in figure 2, has a split second peak like that observed experimentally, which is often thought to be related to the existence of an icosahedron in the system. Although the averaged potential energies per atom of these models are quite different, their structural characteristics are very similar to each other (see table 1). Therefore, it is reasonable that these models reproduce the three metastable states of AMA $Fe_{80}B_{20}$ upon thermal annealing. Accordingly, the lowest energy model corresponds to a well-relaxed and the highest energy model to an as-quenched specimen.

Table 2 lists the number of bubbles detected in our models. All models contain more than one bubble per atom. The well-relaxed model (model C) has a smaller number of bubbles compared to the as-quenched model (model A). This trend is

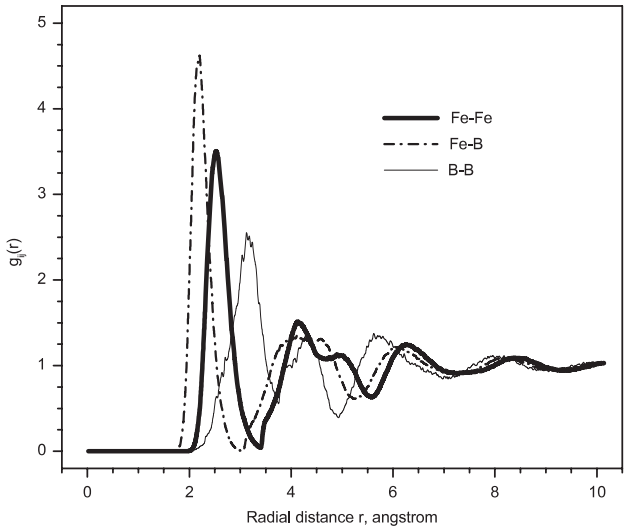

Figure 2. The pair distribution functions of model A.

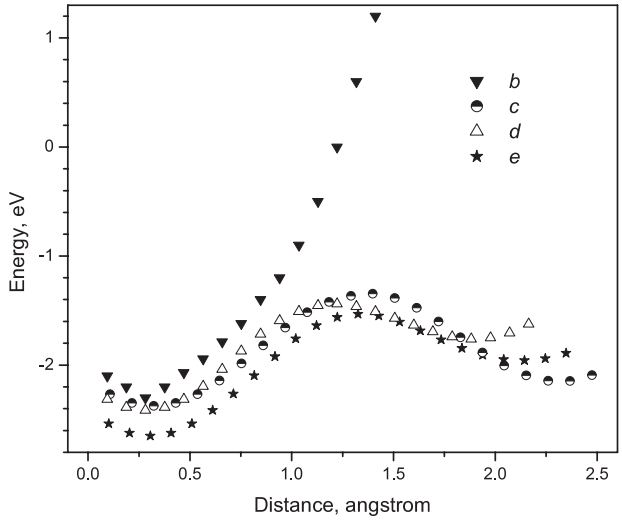

Figure 3. Potential energy profile of atoms moving from their site to the center of the CST; (c)–(e) belong to VB.

Table 1. Structural characteristics of the amorphous alloy $Fe_{80}B_{20}$. Here r_{FeFe}, r_{FeB} and r_{BB} are the positions of the first peak in the PDFs for pair Fe–Fe, Fe–B and B–B respectively; Z_{FeFe}, Z_{FeB}, Z_{BFe} and Z_{BB} are the averaged coordination number for pairs Fe–Fe, Fe–B, B–Fe and B–B, respectively.

	r_{FeFe} (Å)	r_{FeB} (Å)	r_{BB} (Å)	Z_{FeFe}	Z_{FeB}	Z_{BFe}	Z_{BB}
Model A	2.52	2.2	3.12	11.64	2.34	9.35	4.30
Model B	2.54	2.18	3.20	11.66	2.35	9.39	4.32
Model C	2.54	2.18	3.18	11.69	2.36	9.45	4.35
$Fe_{80}B_{20}^{a}$	2.65	2.20	3.15	—	—	—	—
$Fe_{80}B_{20}^{a}$	2.57	2.14	—	12.4	2.2	8.6	—
$Fe_{80}B_{20}^{a}$	2.57	2.06	—	11.8	2.4	9.3	—
$Fe_{83}B_{17}^{a}$	2.58	2.1	—	12.2	1.9	9.4	—

[a] The experimental data from [26–28].

Table 2. The number of bubbles.

Model	The mean potential energy per atom	Number of atoms n_B 5	6	7	8	9
A	−1.4889	102 615	17 580	823	64	0
B	−1.4995	100 029	15 843	879	67	1
C	−1.5195	97 235	15 195	546	8	0

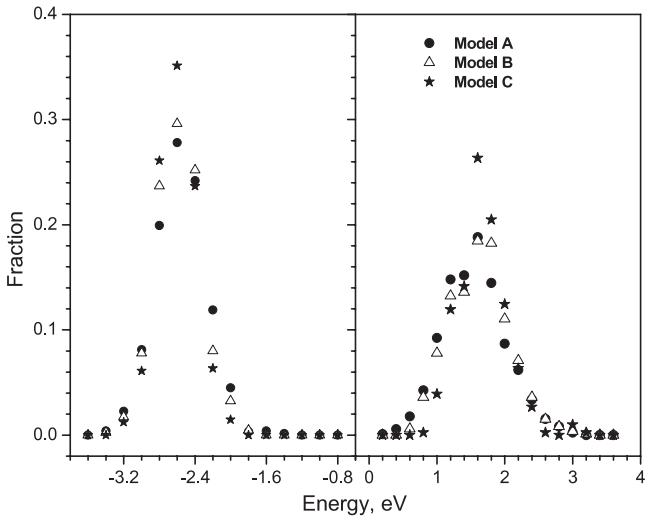

Figure 4. The distributions of site energy (left) and energy barrier (right) for DAs.

also observed in table 3 showing the distribution of bubble radius. It can be seen that the number of large bubbles, those with a radius larger than 1.6 Å, in the well-relaxed model is smaller than that in the less-relaxed model. In model A we found more than 20 bubbles with a radius close to the lattice constant of bcc crystal iron (∼2.86 Å).

Now we focus on the question of the importance of the bubbles for diffusion. For every bubble, we examine the potential energy variation of all neighboring atoms as they move step by step on a line connecting their initial equilibrium position and the center of the CST. The length of the displacement step is equal to 0.02 Å (see figure 1(b)). The potential energy profiles (PEP) for an atom moving into the bubbles b, c, d and e are shown in figure 3. For the bubble b, a monotonous increase is found. It means that the neighboring atom cannot jump into bubble b due to a very large energy barrier. In the case of the bubbles c, d and e we conversely observe a maximum in the graph of the PEPs. These are like the typical PEP for a tracer atom jumping into a vacancy. Therefore, these bubbles play a role as a diffusion defect like a vacancy in crystal. Hereafter, we call the bubbles shown in figure 3 having the PEPs c, d and e, vacancy bubbles (VB). The atoms attaining the corresponding PEP are called the diffusing atom (DA). The numbers of VBs are listed in table 4. There are two kinds of VB: iron-VB, where the Fe atom can move into the VB and boron-VB corresponding to the boron-DA. It is essential to notice that in the less-relaxed model the number of both kinds of VB is larger compared to the well-relaxed model. Furthermore, the ratio m_{Fe}/m_B for the less-relaxed model is also larger compared to the well-relaxed model. Figure 4 shows the distributions of site energy and the energy barrier for the DA. The graphs for all models considered are similar

Table 3. The distribution of bubble radius.

R_B (Å)	1.4	1.5	1.6	1.7	1.8	1.9	2	2.1	2.2	2.3	>2.4
Model A	270	22 725	27 516	30 039	29 840	6729	2751	918	203	71	20
Model B	211	23 225	27 260	28 717	29 229	5305	2090	655	104	23	0
Model C	216	25 329	25 503	28 299	28 417	4000	1046	169	5	0	0

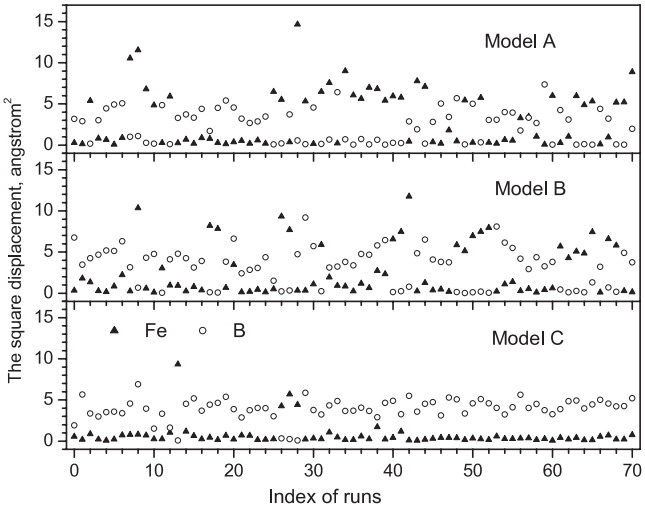

Figure 5. The square displacements of iron and boron atoms x^2_{Fei}, x^2_{Bi} for the ith run of DA moving; $i = 1, 2, \ldots, 70$.

to each other and have a Gaussian form. The energy barrier is determined by the difference between the maximum point in the PEP and the site energy of the DA (see figure 3).

After the determination of VBs we displace the DA into the center of the CST and then relax the system until it reaches a new equilibrium, in order to inspect the collective atomic movement. For convenience we call the simulation procedure just described 'the DA moving'. Table 4 lists the averaged square displacements $\langle x^2_{Fe}\rangle$, $\langle x^2_B\rangle$ after the DA moving is completed, and the x^2_{Fei}, x^2_{Bi} for the individual ith run is displayed in figure 5. It clearly shows that the x^2_{Bi} mostly fluctuates around 4.0 Å^2 for boron-DA and it is close to zero in the case of iron-DA. Because the jumping distance of the DAs is in the range of 1.7–1.9 Å, it follows that the boron-DA contributes the dominant part of x^2_{Bi} e.g. other B atoms move not so far from their initial positions under the DA moving. In model A we sometimes observe very large x^2_{Bi} (>7 Å^2) indicating several B atoms involved in the collective motion. In the case of iron-DA the value of x^2_{Fei} for most runs is conversely significantly larger than 4.0 Å^2 and sometimes it reaches ∼16 Å^2. This result is expected and shows the collective character of the atomic movement upon iron-DA moving. Due to its large size in comparison with boron, the jump of an iron atom leads to a significant local rearrangement of the atoms located near the VB. Meanwhile, small boron diffuses like the movement of an interstitial impurity through the boron bubbles.

As such, the diffusion mechanism is performed as follows: one DA (B or Fe) jumps into a VB and the present VB disappears, but another VB may be created somewhere in an amorphous matrix due to the collective atomic movement upon DA moving. The most probable place for the formation of a new VB is the location where the bubbles exist. It means, that as a result of collective movement of a group of atoms, the bubbles become VBs. That is, the VB is unlike the quasi-vacancy described in [1–5] which moves over a certain distance until it is annihilated at a sink source (free surface, internal cavity).

Table 4. The number of VBs and the averaged square displacement upon the DA moving. Here $\langle x^2_{Fe}\rangle$, $\langle x^2_B\rangle$ are the averaged square displacement of Fe and B atoms as a DA jumps into the VB respectively; m_{Fe}, m_B are the numbers of iron- and boron-VB, respectively.

			Iron-DA		Boron-DA	
Model	m_{Fe}	m_B	$\langle x^2_{Fe}\rangle$ (Å^2)	$\langle x^2_B\rangle$ (Å^2)	$\langle x^2_{Fe}\rangle$ (Å^2)	$\langle x^2_B\rangle$ (Å^2)
A	472	772	7.140	0.508	0.613	4.092
B	234	627	6.482	0.251	0.758	4.478
C	28	382	5.664	0.321	0.447	4.171

Consider jumps of the ith DA with the jump completion frequency φ_i and the mean square displacement x^2_{Si} for S-type atoms, the diffusion coefficient [33]

$$D_s = \tfrac{1}{6} f \langle \varphi_i x^2_{Si}\rangle, \tag{2}$$

where S denotes Fe or B; f is the correlation factor for consecutive hops. The averaging $\langle \varphi_i x^2_{Si}\rangle$ must be carried over all ith atoms. We thus get

$$\langle \varphi_i x^2_{Si}\rangle = \frac{1}{N_{Atom}}\left[\sum_i^{m_{Fe}} \varphi_{Fei} x^2_{Si} + \sum_i^{m_B} \varphi_{Bi} x^2_{Si}\right]. \tag{3}$$

The jump frequency φ_{Si} is given as

$$\varphi_{Si} = \nu_0 \exp(s_{mSi}/k_B)\exp(-h_{mSi}/k_B T) \approx \nu_0 \exp(-h_{mSi}/k_B T). \tag{4}$$

Here s_{mSi}, h_{mSi} denotes the entropy change and migration enthalpy; k_B is the Boltzmann constant; T is the temperature; ν_0 is the attempt frequency (∼10^{12} s^{-1}).

There is only a small amount of experimental data on tracer diffusion in the $Fe_{80}B_{20}$ system, so we make a comparison with the amorphous alloy $Fe_{40}N_{40}B_{20}$, which has very accurate data on tracer diffusion. From the data shown in table 4 and figure 3, we get $D_{Fe} = 10^{-20}$–5×10^{-22} and $D_B = 10^{-19}$–2×10^{-19} m^2 s^{-1} at 593 K. This result is consistent with experimental data for amorphous $Fe_{80}B_{20}$ ($D_{Fe} \sim 10^{-21}$–10^{-22} m^2 s^{-1} [1]) and $Fe_{40}N_{40}B_{20}$ ($D_{Fe} \sim 10^{-21}$ and $D_B \sim 10^{-19}$ m^2 s^{-1} [29–31]) at the temperature considered. As regards the relaxation effect, our simulation shows that the decrease in diffusion coefficient results in the loss of VBs upon

relaxation. The numbers of iron- and boron-VBs in model B decreases by factor of 9 and 2 compared to model C (see table 4). As a consequence the diffusion coefficient decreases by a factor of 10 and 3. This result is also in reasonable agreement with experiments on Fe diffusivity in $Fe_{80}B_{20}$ and $Fe_{40}N_{40}B_{20}$ AMA [3, 29–31]. Note that the annihilation of VBs in the well-relaxed model is concerned with the atomic rearrangement within the amorphous matrix, but not due to the sink source where the diffusion effect moves to, which has been described by quasi-vacancy models in previous references (see [1–5]).

4. Conclusion

A systematic study on the diffusion mechanism in amorphous solids has been carried out using three models $Fe_{80}B_{20}$. Several conclusions can be made as follows.

(i) We found that the AMAs have a large number of VBs which could be a diffusion vehicle as a vacancy in crystal i.e. one DA in the VB could move into the center of the CST and present an elemental diffusion jump. The number of VBs are found in the range from 4.1×10^{-3} to 1.245×10^{-2} per atom for AMA $Fe_{80}B_{20}$ depending on the degree of relaxation.

(ii) We present a new diffusion mechanism in that a DA jumps into the VB, then the collective movement of neighboring atoms starts. Consequently, the present VB disappears, but another VB may be created elsewhere in the amorphous matrix. The diffusion coefficients of B and Fe are calculated via the VBs detected and the result is very consistent with experimental data, indicating the validity of the suggested diffusion mechanism.

(iii) The decrease in diffusivity upon the relaxation found in the present work results in VB annihilation. Our simulation reveals that the VB is unlike the quasi-vacancy, which is used to interpret the relaxation effect in previous works. The VB annihilation relates to a DA jump into the VB and the atomic rearrangement within the amorphous matrix occurring under the DA moving completed. The most probable place for the formation of a new VB upon DA moving is a location where bubbles exist.

Acknowledgment

This work was supported financially by NAFOSTED of the Ministry of Science and Technology Vietnam (Grant No. 103.01.32.09).

References

[1] Horvath J, Ott J, Pfahler K and Ulfert W 1988 *Mater. Sci. Eng.* **97** 409
[2] Frank W *et al* 1988 *Mater. Sci. Eng.* **97** 415
[3] Tyagit A K, Macht M P and Naundorf V 1991 *Acta Metall. Mater.* **39** 609
[4] Frank W, Horner A, Scharwaechter P and Kronmiiller H 1994 *Mater. Sci. Eng.* A **179/180** 36
[5] Schuler T 1995 *NanoStruct. Mater.* **6** 863
[6] Flege S, Fecher U and Hahn H 2000 *J. Non-Cryst. Solids* **270** 123
[7] Griesche A 2004 *Mater. Sci. Eng.* A **375–377** 285
[8] Chakravarty S *et al* 2009 *Acta Mater.* **57** 1263
[9] van den Beukel A and Sietsma J 1991 *Mater. Sci. Eng.* A **134** 935
[10] Sharma S K *et al* 1988 *Acta Metall.* **36** 1683
[11] Kijek M 1980 *Scr. Metall.* **14** 1337
[12] Duine P A, Wonnell S K and Sietsma J 1994 *Mater. Sci. Eng.* A **179/180** 270
[13] Roos W D *et al* 1990 *Appl. Surf. Sci.* **40** 303
[14] Limoge Y 1990 *J. Non-Cryst. Solids* **117/118** 708
[15] Ruitenberg G, de Hey P, Sommer F and Sietsma J 1997 *Mater. Sci. Eng.* A **226–228** 397
[16] Limoge Y 1990 *Acta Metall. Mater.* **38** 1733
[17] Limoge Y and Brebec G 1988 *Acta Metall.* **36** 665
[18] Averback R S 1991 *MRS Bull.* **16** 47
[19] Limoge Y 1997 *Mater. Sci. Eng.* A **226–228** 228
[20] Hung P K, Hue H V and Vinh L T 2006 *J. Non-Cryst. Solids* **352** 3332
[21] Zhu A, Shiflet G J and Poon S J 2008 *Acta Mater.* **56** 3550
[22] Leon D *et al* 1997 *Mater. Sci. Eng.* A **226–228** 296
[23] Naundorf V *et al* 1998 *J. Non-Cryst. Solids* **224** 122
[24] Kronmuller H, Frank W and Horner A 1991 *Mater. Sci. Eng.* A **133** 410
[25] Van Hoang V 2004 *J. Phys. B: At. Mol. Opt. Phys.* **348** 347
[26] Lamparter P *et al* 1981 *Z. Naturforsch.* **6** 165
[27] Hirata A, Hirotsu Y, Ohkubo T, Hanada T and Bengus V Z 2006 *Phys. Rev.* B **74** 214206
[28] Nold E, Lamparter O, Olbrich H, Rainer-Harbach G and Steeb S Z 1981 *Naturfors. Teil* A **36** 1032
[29] Horvath J and Mehrer H 1986 *Cryst. Latt. Deft Amorph. Mater.* **13** 1
[30] Ulfert W, Horvath J, Frank W and Kronmfiller H 1989 *Cryst. Latt. Deft Amorph. Mater.* **18** 519
[31] Calm R W, Evetts J E, Patterson J, Somekh R E and Kenway Jackson C 1980 *J. Mater. Sci.* **15** 702
[32] Press W H, Teukolsky S A, Vetterling W T and Flannery B P 1992 *Numerical Recipes* (New York: Cambridge University Press)
[33] Mehrer H 2007 *Diffusion in Solids* (Berlin: Springer)